

Laure S. Fournier  
Charles Andre Cuenod  
Cedric de Bazelaire  
Nathalie Siauve  
Christophe Rosty  
Phuong Lan Tran  
Guy Frija  
Olivier Clement

## Early modifications of hepatic perfusion measured by functional CT in a rat model of hepatocellular carcinoma using a blood pool contrast agent

Received: 17 April 2003  
Revised: 17 October 2003  
Accepted: 16 March 2004  
Published online: 29 July 2004  
© Springer-Verlag 2004

L. S. Fournier (✉) · C. A. Cuenod  
C. de Bazelaire · N. Siauve · G. Frija  
O. Clement  
Laboratoire de Recherche en Imagerie,  
INSERM U494, Necker Institute,  
156 rue de Vaugirard, 75015 Paris, France  
e-mail: lfd@free.fr  
Tel.: +33-1-56093841  
Fax: +33-1-56093850

C. Rosty  
Department of Pathology,  
Hopital Europeen Georges Pompidou,  
20 rue Leblanc, 75015 Paris, France

P. L. Tran  
INSERM U370, Necker Institute,  
156 rue de Vaugirard, 75015 Paris, France

**Abstract** Macromolecular contrast-enhanced functional CT was performed to characterize early perfusion changes in hepatocellular carcinoma (HCC). Fourteen rats with chemically induced primary liver tumors ranging pathologically from hyperplasia to HCC and 15 control rats were investigated. Two dynamic CT scans using an experimental macromolecular contrast agent were performed on a single slice 11 and 18 weeks after tumor induction followed by pathological examination. A deconvolution mathematical model was applied, yielding the hepatic perfusion index (HPI), mean transit time (MTT), liver distribution volume (LDV) and arterial, portal and total blood flows (FA, FP, FT). Analysis was performed on one slice per rat, containing overall two hyperplasia, six dysplasia and 15 HCC. On the first scans, HCC at an early

pathological stage had a low FP (−30%,  $P=0.002$ ) but a normal arterial-portal balance. On the scan contemporary to pathology, HCC perfusion parameters showed an inversion of the arterial-portal balance (HPI +212%,  $P<0.0001$ ), with a high FA (+56%,  $P=0.002$ ) and a low FP (−69%,  $P<0.0001$ ). Sensitivity and specificity of detection of HCC by perfusion CT were high (87 and 80%) on late scans; but also on the earlier scans (86 and 65%), even though only one (7%) was visible to the eye. Perfusion-CT allowed early detection of HCC. This technique could contribute in the detection and characterization of liver lesions in clinical studies.

**Keywords** Angiogenesis · Perfusion imaging · Hepatocellular carcinoma · Computed tomography · Animal imaging

### Introduction

Hepatocellular carcinoma (HCC) is the most frequent primary liver tumor [1]. In Western countries, it occurs mainly in cirrhotic livers [2]. A curative treatment is possible only if it is detected at an early stage [3]. Imaging techniques such as contrast-enhanced MRI or CT allow diagnosis for most HCC over 1 cm (sensitivity of 86–95%) [1]. However, for small HCC, sensitivity is much lower (under 50%). It is therefore important to develop imaging methods that can detect and characterize tumors at an early stage in order to implement a timely treatment.

Tumors need to develop a new vascular network to supply nutrients and oxygen [4]. In the liver, tumors have a predominantly arterial input. This is in contrast to normal tissue, which depends mainly on portal blood [5]. In this study, we applied a perfusion-CT technique using an X-ray blood pool contrast agent allowing a quantification of liver perfusion parameters in order to try to reveal these vascular changes.

We used an HCC model in rats inducing a spectrum of hepatic lesions by means of a chemical carcinogen, diethylnitrosamine (DEN), simulating the type of lesions that can be observed in human liver carcinogenesis [6].

Our team developed an image processing method to measure perfusion after a bolus injection of an experimental macromolecular contrast agent. This technique has been shown to detect occult liver micrometastases in a rat model [7]. Our intent was to demonstrate the existence of alterations in liver microcirculation in HCC and to show that these alterations appeared at an early stage in tumoral development.

## Materials and methods

### Animal model

Institutional committees for animal care approved all animal experiments. Thirty-five male Wistar rats (Iffa Credo, l'Arbesles, France) were used for the experiment. Fifteen of these were healthy male Wistar rats, weighing from 410 to 460 g, used as controls. Twenty male Wistar rats were used for tumor induction, weighing 150 g at the end of the induction, growing to 350–530 g during the 18-week imaging period. HCC was induced in the rats by dissolving diethylnitrosamine (DEN) (Sigma-Aldrich Co., St Louis, MO) in their drinking water (1 g/l), which was given ad libitum for 6 weeks. DEN is a carcinogen inducing liver tissue changes of progressive malignancy. This model produces a variety of lesions such as hyperplasia, dysplasia and HCC. The pathological aspects of these lesions are comparable to those encountered in human primary liver carcinogenesis [8]. In this model, it is hypothesized, as in humans, that dysplastic nodules are precursors to HCC. However, the link between hyperplasia and HCC is more difficult to establish. The relative frequency of each type of lesions is dependent on the dose and the time period of administration of DEN. We chose a protocol with a short 6-week period of induction in order to obtain a majority of lesions at an early stage of tumor development at the beginning of the study.

### Imaging

Before imaging, animals were anesthetized with an intraperitoneal injection of a 50/50 mix of xylazine (10 mg/kg, Rompun, Bayer Pharma, Puteaux, France) and ketamine (50 mg/kg, Imalgene1000, Merial, Lyon, France).

Two perfusion-CT scans were performed 11 and 18 weeks after the end of the induction. The first scans were considered to be performed “early” in tumoral progression, whereas the second scans were considered as “late” in tumoral progression.

**Perfusion-CT imaging.** CT imaging was performed on a Prospeed imager (General Electric, Milwaukee, WI) with the following parameters: acquisition field of view 25 cm, reconstruction field of view 9 cm, 80 kV, 200 mA, matrix 256×256, slice thickness 3 mm and spacing 0 mm, following the technique described in references [7, 9].

The contrast agent was an experimental iodinated macromolecular agent P743 developed by Guerbet (Aulnay-sous-Bois, France) [10, 11]. Its molecular weight was approximately 13 kDa, and its concentration 150 mg of iodine/ml. This contrast agent is a rapid clearance blood pool agent, and its half-life in rats is 4 min. It was injected manually in one of the tail veins at a concentration of 150 mg of iodine/kg. This concentration was chosen according to the results described in reference [10] and was shown to yield a satisfactory enhancement despite being lower than usual clinical doses of iodine (300 mg of iodine/kg).

Rats fasted 8 h before scanning. During CT imaging, the rats were placed in a supine position, and the whole liver was imaged. A single slice containing simultaneously the aorta, portal vein and liver parenchyma was selected. Fifty images were then acquired at

this chosen level during 50 s. A bolus of contrast agent was injected 5 s after the beginning of acquisition. Images were secondarily reconstructed with a 0.3 s temporal resolution, extrapolating to a total of 163 slices over the 50 s.

### Pathology

Rats were sacrificed after the last set of imaging by an intraperitoneal injection of a lethal dosage of sodium pentobarbital (Sanofi, Libourne, France). Their liver was removed and fixed in 20/1 acetic formalin after injecting 0.1 ml of the same solution in the portal vein. A slice was cut at the same level as the slice imaged in CT (using the portal vein as an anatomical reference), embedded in paraffin, and thinner sections of 3  $\mu$ m were cut and stained with hematoxylin-eosin-safran. These slices were examined with an optical microscope, at  $\times 20$  and  $\times 50$  magnification, and lesions of hyperplasia, dysplasia or HCC were noted. The size and location of each lesion were recorded on a diagram and classified according to its pathological state.

On microscopic examination, the lesions were defined as follows:

- “Normal” liver tissue: absence of pathological abnormality
- “Hyperplasia”: well-limited groups of cells organized in thick trabeculae composed of three or four cells instead of a single cell as in normal liver
- “Dysplasia”: limited or diffuse groups of hypertrophied cells with atypical nuclei and cytoplasm, arranged in disorganized trabeculae
- “Hepatocellular carcinoma”: disorganized groups of cells of variable sizes, with enlarged and irregular nuclei, disposed in thickened and anarchic trabeculae or in a pseudo-glandular pattern

### Image processing

**Enhancement curves.** CT images were transferred on a workstation (Advantage Windows, General Electric, Milwaukee, WI). Regions of interest (ROI) were placed on the aorta, portal vein and liver parenchyma. Liver ROI were placed on each location where a lesion of hyperplasia, dysplasia or HCC had been observed on corresponding pathological slices. We also placed ROI on liver parenchyma that did not show any abnormality on pathological examination to represent normal liver tissue. Equivalent ROI were placed on both the early and late scans. For the control animals, two or three ROI were placed randomly on the liver parenchyma of each animal.

A program developed in our laboratory [7, 9] reported the ROI on each slice/time point and measured mean signal intensity of pixels. A graph representing the evolution of signal enhancement of the ROI over time was obtained. For a detailed description of the model and the equations defining the parameters, see references [7, 9].

**Deconvolution model.** Liver tissue was considered as a double-input system (hepatic artery and portal vein) to take into account the dual hepatic perfusion with a single output (hepatic veins). The deconvolution algorithm allowed the calculation of six parameters quantifying perfusion for each tissue ROI:

- (a) Hepatic perfusion index, which is the percentage of total blood flow of arterial origin, expressed in %
- (b) Mean transit time, which is the mean time taken by molecules of contrast agent to flow through the system, expressed in seconds
- (c) Liver distribution volume, which is the percentage of tissue volume in which the contrast agent distributes itself, expressed in % or ml/cc of tissue
- (d) Arterial, portal and total blood flow ( $F_A$ ,  $F_P$ ,  $F_T$ ), which are fractional blood flows, expressed in ml/min/cc of tissue

## Statistical analysis

All results are given by mean  $\pm$  standard deviation. Control vs. DEN-treated rats were compared by unpaired Student's *t*-test.  $P \leq 0.05$  was considered as statistically different. An analysis of variance among groups of DEN-treated rats was performed with a Bonferroni–Dunn test, comparing effects of time (early vs. late scan) and pathology (normal, hyperplasia, dysplasia and HCC).

Sensitivity and specificity for detection of HCC with perfusion CT were determined for the early and late stage of the tumoral process. For perfusion CT, the criteria used were values of  $HPI > 40\%$ ,  $MTT < 12.5$  s,  $LDV < 37.5\%$ ,  $F_T < 2.25$  ml/min/cc,  $F_A > 0.70$  ml/min/cc and  $F_P < 1.00$  ml/min/cc, using pathology as the gold standard. These values were chosen to optimize the sensitivity and specificity of HCC detection in our study.

## Results

### Pathological findings

Out of 20 rats presenting tumors, four died spontaneously of their disease before we could complete the study, and two died as a result of the anesthesia at the time of imaging. Fourteen rats therefore underwent the complete protocol.

Diameters of the lesions were estimated on microscopic examination of the single slice corresponding to the CT slice and ranged from 1 to 15 mm. Eleven tumors measured less than 5 mm, two measured between 5 and 10 mm, and two measured between 10 and 15 mm. There were no signs of underlying liver fibrosis or cirrhosis.

A total of 36 areas in the 14 rats were identified by microscopical examination of the single slice corresponding to the CT slice. Thirteen were normal, two were hyperplasia, six were dysplasia, and 15 were HCC. They were subsequently and retrospectively reported as corresponding ROI on CT scans. One ROI corresponding to an HCC could not be reported on the early scan, since its area of liver was artifacted due to gut movement. Tumoral vessels were thin and tortuous, appearing similar to capillaries, with a continuous endothelial lining, in contrast to normal liver sinusoids. Some HCC had large, more or less confluent vascular “lakes” with or without an endothelial lining. Others had necrotic or hemorrhagic zones with no recognizable vessel. Some cells had clear or fatty inclusions, or contained Mallory’s bodies. Figure 1 illustrates the microscopic aspect of hyperplasia, dysplasia and HCC.

### Perfusion scan imaging findings

**Imaging results.** Neither hyperplasia nor dysplasia lesions were visible on CT in our study. Only 1 out of 14 HCC was visible on the first scan (7%), and 8 out of 15 on the second (53%). Three qualitatively different enhancement profiles were observed on the second scan: two tumors were heterogeneous and did not enhance after injection, four had a low signal compared to the sur-

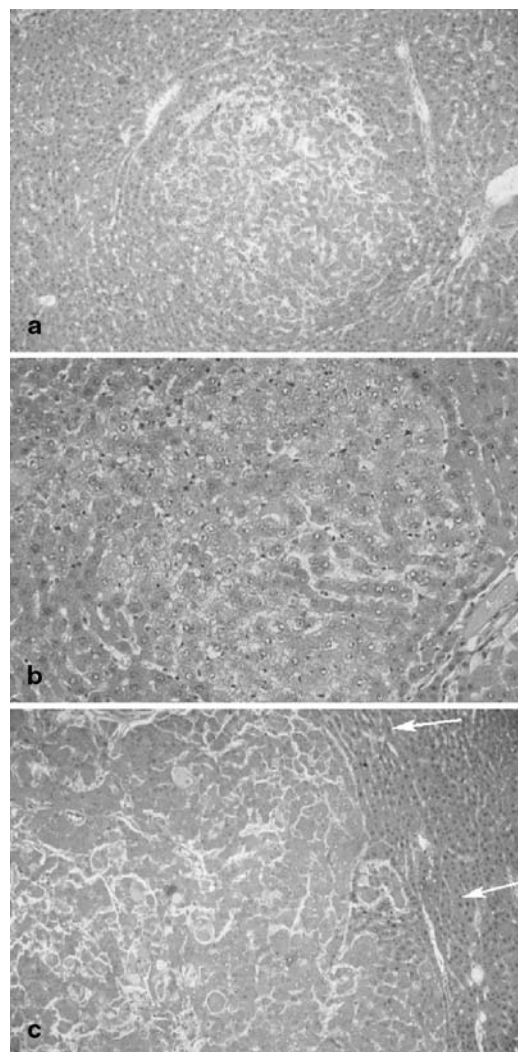


**Fig. 1** Pathology. Microscopical examination of liver lesions: **a** hyperplasia, **b** dysplasia, **c** HCC. Hematoxylin, eosin and safran staining,  $\times 20$  magnification for **a**, **c**,  $\times 50$  for **b**. Arrows delineate the limit between normal parenchyma and the lesion

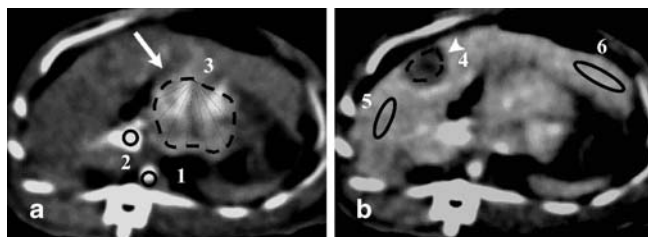


**Fig. 2** Contrast-enhanced CT in a rat 18 weeks after tumor induction. Axial images acquired **a** 11 s and **b** 20 s after injection of macromolecular contrast media. **a** On the images acquired during the arterial phase, one of the HCC (arrow) enhances intensely, whereas **b** another HCC is visible only at the portal phase (arrow-head) as a lesion of decreased signal compared to adjacent normal liver. On these images, ROI were placed with the TIFON software, represented by black lines on the aorta (1), the portal vein (2), the two HCCs (3 and 4), and two zones with no visible pathological abnormality on the corresponding microscopic slice (5 and 6)

**Fig. 3** Representative enhancement curves. Evolution of signal intensity over time measured in the ROI placed on the aorta, the portal vein, and two examples of normal liver parenchyma. Signal intensity first rose in the aorta, with a peak at 9 s, then in the portal vein, with a peak at 12 s. At the equilibrium phase, signal intensities in these vessels were equal. HU, Hounsfield units

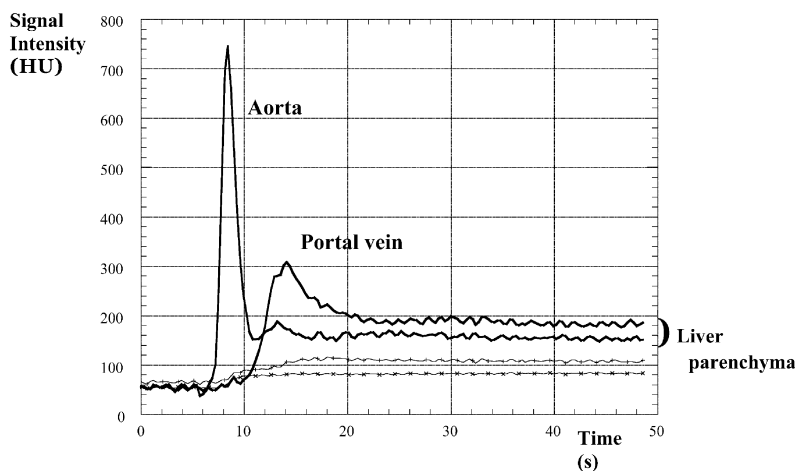


**Table 1** Perfusion parameters on the early scan performed 11 weeks after the beginning of the tumor induction and 7 weeks before pathology

Histology	Control (n=43)	Normal (n=13)	Hyperplasia (n=2)	Dysplasia (n=6)	HCC (n=14)
HPI (%)	18.6±9.6	18.2±14.0	4.9±2.1	8.2±6.7*	19.3±25.3
MTT (s)	9.9±2.1	9.7±2.6	7.2±0.8	9.2±2.0	11.5±3.4*
LDV (%)	43.9±6.8	37.5±5.8*	36.1±2.6	33.8±2.8*	34.3±7.8*
$F_T$ (ml/min/cc)	2.72±0.77	2.39±0.40	3.00±0.17	2.28±0.48	1.87±0.43*
$F_A$ (ml/min/cc)	0.50±0.26	0.42±0.09	0.14±0.05	0.17±0.15*	0.28±0.28*
$F_P$ (ml/min/cc)	2.27±0.67	1.96±0.52	2.85±0.23	2.10±0.49	1.58±0.62*

The histology of the ROI was that observed when histology was performed at the end of the experiment. Results statistically different from controls ( $P \leq 0.05$ ) are noted with an asterisk. One ROI corresponding to an HCC could not be reported on the early scan, since its area of liver was artifacted due to gut movement.

HPI, hepatic perfusion index; MTT, mean transit time; LDV, liver distribution volume;  $F_T$ , total blood flow;  $F_A$ , arterial blood flow;  $F_P$ , portal blood flow.

**Table 2** Perfusion parameters on the late scan performed 18 weeks after the beginning of the tumor induction and immediately before pathology

Histology	Control (n=43)	Normal (n=13)	Hyperplasia (n=2)	Dysplasia (n=6)	HCC (n=15)
HPI (%)	18.6±9.6	23.5±17.2	10.2±2.4	46.1±31.7*	58.1±28.3*
MTT (s)	9.9±2.1	10.4±2.1	10.0±0.7	13.9±6.6*	15.2±4.3*
LDV (%)	43.9±6.8	37.0±4.2*	39.4±0.4*	41.0±6.3	35.5±6.3*
$F_T$ (ml/min/cc)	2.72±0.77	2.19±0.46*	2.35±0.15*	2.06±0.79	1.50±0.42*
$F_A$ (ml/min/cc)	0.50±0.26	0.53±0.43	0.24±0.07	0.76±0.36*	0.78±0.35*
$F_P$ (ml/min/cc)	2.27±0.67	1.66±0.47*	2.11±0.08	1.29±0.91*	0.71±0.64*

Results statistically different from controls ( $P \leq 0.05$ ) are noted with an asterisk.

HPI, hepatic perfusion index; MTT, mean transit time; LDV, liver distribution volume;  $F_T$ , total blood flow;  $F_A$ , arterial blood flow;  $F_P$ , portal blood flow.

rounding liver parenchyma, and two were heterogeneous with an early and intense enhancement (Fig. 2).

**Enhancement curves.** Contrast agent was injected 5 s after the beginning of the acquisition. All imaging sessions yielded satisfactory enhancement curves (Fig. 3). A representative curve presented an aortic enhancement beginning at 7 s with a peak at 9 s, followed by a portal enhancement beginning at 10 s with a peak at 12 s. These delays and the height of signal peaks (700–800 HU for

the hepatic artery, 250–350 HU for the portal vein) varied little from animal to animal. As expected, aortic and portal enhancements were equal at the stationary phase.

**Perfusion parameters.** The software did not fail in the analysis of any of the ROI, including for the lesions that appeared cystic or hemorrhagic on microscopic examination.

Tables 1, 2 present mean results of perfusion parameters measured, respectively, on the first and second scan, according to the pathological type.



**Table 3** Perfusion parameter changes according to pathology

	'Normal'		Dysplasia	HCC	Dysplasia	HCC
	Early	Late	Early	Early	Late	Late
HPI			↘		↗	↗↗
MTT				↗	↗	↗
LDV	↘	↘	↘	↘		
$F_T$		↘		↘		↘↘
$F_A$			↘	↘	↗	↗↗
$F_p$		↘		↘		↘↘

Results for hyperplasia were not presented since there were only two ROI. 'Normal' represented regions of liver parenchyma showing no pathological abnormality. Only statistically significant changes compared to controls were represented in this table. HCC, hepatocellular carcinoma; HPI, hepatic perfusion index; MTT, mean transit time; LDV, liver distribution volume;  $F_T$ , total blood flow;  $F_A$ , arterial blood flow;  $F_p$ , portal blood flow.

These were compared to the mean results of control rats with an unpaired Student's *t*-test. Statistically significant differences are indicated in the tables by an asterisk.

The Bonferroni-Dunn test showed a significant difference for DEN-treated rats between the early and late scans for all the parameters except LDV. Table 3 combines results according to pathological type and early/late stage, representing the increase or decrease of the perfusion parameter compared to controls.

Whether on the early or on the late scan, all ROI showed a statistically ( $P=0.001$ ) lower distribution volume and total blood flow ( $P=0.020$ ), respectively,  $-7$  to  $-19\%$  and  $-12$  to  $-45\%$ , relative to controls, including those that showed no abnormality on pathology (classified as normal).

Due to the low number of hyperplastic ROI, no specific conclusion could be drawn from their results.

For the dysplastic ROI, the early scan also showed a decrease in HPI ( $-56\%$ ,  $P=0.014$ ), because of a decrease in arterial blood flow ( $-66\%$ ,  $P=0.006$ ). On the later scan, there was an inversion of the arterial-portal balance, with an HPI on the contrary elevated ( $+148\%$ ,  $P<0.0001$ ) because of a combined increase in arterial blood flow and decrease in portal blood flow. Dysplastic lesions also presented an increase in MTT ( $+140\%$ ,  $P=0.004$ ).

On the early scan, HCC had a perfusion profile that seemed intermediate between early and late dysplastic ROI. They had a decrease in arterial blood flow ( $-44\%$ ,  $P=0.013$ ) like early dysplasia, as well as an increase in MTT ( $+16\%$ ,  $P=0.046$ ) and decrease in portal blood flow ( $-30\%$ ,  $P=0.002$ ) such as was observed in late dysplasia. However, their HPI was normal (it was decreased in the early and increased in the late dysplasia). On the later scan, the perfusion changes noted for HCC were similar, but more massive than those in late dysplastic ROI. There was an inversion of the arterial-portal balance (HPI  $+212\%$  compared to normal ROI,  $P<0.0001$ ), combining a strong increase in arterial ( $+56\%$ ,  $P=0.002$ ) and a strong decrease in portal blood flows ( $-79\%$ ,  $P<0.0001$ ). The increase in MTT was also observed ( $+54\%$ ,  $P<0.0001$ ).

Figures 4 and 5, respectively, show the changes in HPI and MTT between the control rats and the early and late perfusion CT of each pathological type of lesion. The Bonferroni-Dunn test showed significant differences between early and late scans ( $P<0.0001$  for HPI and  $P=0.002$  for MTT) and between normal ROI and HCC ( $P=0.002$  for HPI and  $P=0.001$  for MTT). MTT and HPI were increased in DEN-induced rats compared to controls, seeming proportional to the pathological grade of

**Fig. 4** HPI mean values of control rats and carcinoma-induced rats at the early and late stage of carcinogenesis. The HPI was similar to the control rats in "pathologically normal" liver tissue and did not change over time. For hyperplastic tissue, the HPI was lower than controls, as well as for early dysplastic tissue. The most important change in HPI was for "late-stage" HCC and dysplasia, which was very elevated compared to controls

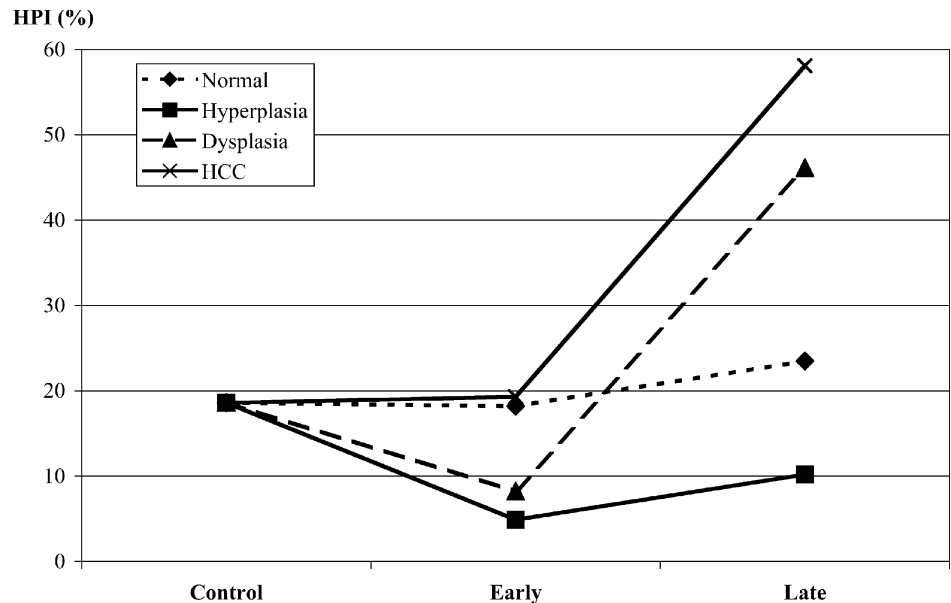


**Fig. 5** MTT mean values of control rats and carcinoma-induced rats at the early and late stage of carcinogenesis. The MTT was similar to the control rats in “pathologically normal” liver tissue and did not change over time. For hyperplastic tissue, the MTT decreased at the early stage of evolution. In dysplastic and HCC tissues, MTT increased significantly compared to control values at the late stage, but was already significantly elevated at an early stage for HCC

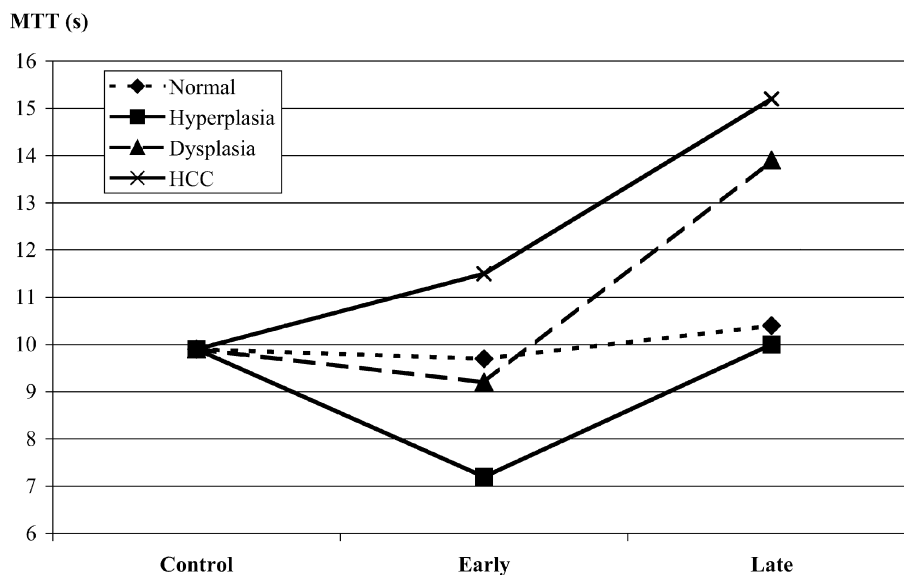


**Table 4** Sensitivity and specificity based on perfusion-CT parameters to predict HCC occurrence 7 weeks before pathological examination. The 20 negative lesions were the ROI that were not

HCC (including normal). One ROI corresponding to an HCC could not be reported on the early scan, since its area of liver was artifacted by gut movement

	Early perfusion CT					
	HPI>40 (%)	MTT>12.5 (s)	LDV<37.5 (%)	$F_T$ <2.25 (ml/min/cc)	$F_A$ >0.70 (ml/min/cc)	$F_P$ <1.00 (ml/min/cc)
Sensitivity	7% (1/14)	29% (4/14)	64% (9/14)	86% (12/14)	14% (2/14)	7% (1/14)
Specificity	100% (20/20)	85% (17/20)	65% (13/20)	65% (13/20)	60% (12/20)	100% (20/20)

HPI, hepatic perfusion index; MTT, mean transit time; LDV, liver distribution volume;  $F_T$ , total blood flow;  $F_A$ , arterial blood flow;  $F_P$ , portal blood flow.

**Table 5** Sensitivity and specificity for HCC detection based on perfusion CT. The 20 negative lesions were the ROI that were not HCC (including normal)

	Late perfusion-CT					
	HPI>40 (%)	MTT>12.5 (s)	LDV<37.5 (%)	$F_T$ <2.25 (ml/min/cc)	$F_A$ >0.70 (ml/min/cc)	$F_P$ <1.00 (ml/min/cc)
Sensitivity	73% (11/15)	80% (12/15)	67% (10/15)	93% (14/15)	67% (10/15)	87% (13/15)
Specificity	75% (15/20)	75% (15/20)	50% (10/20)	40% (8/20)	65% (13/20)	80% (16/20)

HPI, hepatic perfusion index; MTT, mean transit time; LDV, liver distribution volume;  $F_T$ , total blood flow;  $F_A$ , arterial blood flow;  $F_P$ , portal blood flow.

lesions. They increased gradually from normal and hyperplastic tissues to dysplasia to carcinoma, implying a possible predictive role of these parameters to reflect the severity of the lesions.

**HCC detection**

The purpose was to determine if our technique could allow to differentiate HCC from the other lesions based on perfusion parameter values.

Cutoff values for each parameter were chosen to optimize the sensitivity and specificity of HCC detection with our method. Tables 4 and 5 evaluate perfusion CT’s sensitivity and specificity in detecting HCC, respectively, on the first and second set of images, using pathological results as reference.

In Table 4, perfusion CT was performed 7 weeks before pathology. It is difficult to speculate on the nature of the lesions at this early stage, but we can assume that they represented their pathological precursors. A decrease of total blood flow was detected in 12/14 (86%) of the ROI

that would later be revealed to be HCC on pathology. This decrease was due to the decrease in portal blood flow, without an increase in arterial blood flow (which will characterize HCC on the late scan). It is important to state that only one of these HCC was detectable when visually analyzing the dynamic CT acquisition.

Table 5 shows the results of the scans performed immediately before pathology, therefore representing perfusion changes of HCC. Perfusion CT had high sensitivity (73–87%) and specificity (75–80%) when considering parameters such as HPI, MTT and  $F_p$ . Only half of these HCC were visually detectable.

## Discussion

Our results have shown that HCC present specific changes in perfusion parameters compared to normal liver, as measured by our technique of macromolecular contrast-enhanced dynamic CT, even at an early pathological stage.

Control rats were used as a reference for perfusion parameters in normal liver tissue, and our results were consistent with parameters determined in other studies. Conway [12] studied microcirculation in perfused rat livers treated with DEN and also found a perfusion index of approximately 20% (mean of 18.6% in our study) and a blood volume of approximately 40% in normal tissue (mean of 43.9% in our study).

### Histopathological basis for perfusion changes

The lower distribution volume and total blood flow noted for all types of ROI in rats induced by DEN could be explained by a diffuse effect of the carcinogen on the liver. It is possible that DEN induced fibrosis in liver [8], though we did not see any evidence of this on pathological examination. Other groups have also shown a decrease of LDV of macromolecular contrast agents in liver fibrosis [13]. Liver vessels differ from those in most other organs because normal liver sinusoids have a discontinuous base membrane and communicate by large pores with the space of Disse [14]. Therefore, macromolecular contrast agents diffuse instantaneously into this space. The resulting distribution volume included the space of Disse as well as the vascular space. Tumoral liver vessels, on the other hand, have small pores compared to sinusoids and a continuous base membrane (thickened in case of fibrosis) [14] and the contrast agent does not cross the endothelial lining during the short time of observation (50 s). The distribution volume measured is therefore lower since it encompassed only the vascular space. This phenomenon is called capillarization and has been described in this rat model of HCC by Yamamoto [14], and also in human HCC [15].

The marked increase in perfusion index and MTT noted in this study in HCC compared to controls is also consistent with what is known in pathology about HCC vascularization. Tumoral vessels are often irregular and tortuous, which can explain a higher transit time [16]. HCC have a predominantly arterial input, compared to normal liver, which has a predominantly portal input [5]; this characteristic allows detection of HCC in radiological practice. These findings are also observed in rats in Yamamoto's study of rat HCC vessels [14].

If we compare the different pathological stages, two types of perfusion profiles can be distinguished. On one hand, normal and hyperplastic ROI both present a lower distribution volume and total blood flow (with a lower portal blood flow) than controls. On the other hand, dysplastic ROI and HCC not only show a lower distribution volume and total and portal blood flow, but also an increase in the perfusion index, partially because of an increase in arterial input, but more importantly to a decrease in portal input. Normal and hyperplastic zones can be considered as benign states. Dysplasia and HCC are, in contrast, pre-malignant and malignant states [17]. Perfusion CT therefore seems to be able to differentiate benign from malignant pathological states according to their perfusion profiles. The arterialization of vessels (predominantly arterial input compared to liver sinusoids) present even in pre-malignant dysplastic nodules seems to indicate that tumoral transformation of vessels occurs early in the tumor's development. This confirms Folkman's hypothesis that tumors do not develop over a few mm<sup>3</sup> without a simultaneous neoangiogenic process, essential to malignant transformation [4].

In summary, if we wished to speculate on a timeline of changes in perfusion parameters as detected by our technique of perfusion CT and as induced by DEN, it would be as follows. Early diffuse changes occurred first (capillarization), inducing a decrease in LDV. Then followed a decrease in blood flow because of a decrease in the arterial input (early stage dysplasia), then a decrease in portal blood flow and an increase in MTT (early stage HCC). The inversion of the arterial-portal balance (arterialization) in favor of the arterial input occurred secondarily, discreetly in late phase dysplasia, and massively in late phase HCC.

### HCC detection

For the early phase perfusion CT, total blood flow was the best parameter to detect regions "that were to become HCC" 7 weeks later, with a sensitivity of 86%. This was probably due to our method of calculation of total blood flow ( $F_T = LDV/MTT$ ). In early HCC, an association of a decrease in volume and an increase in MTT is observed. Neither parameter was very sensitive by itself, but their combined variations as total blood

flow probably increased sensitivity. HPI, arterial and portal blood flow were not discriminating in detecting "HCC-to-be," which seems to indicate that changes in tumoral vessels such as capillarization (reflected in the decrease of distribution volume) precede arterialization (reflected in the increase of arterial blood flow and HPI).

### Limitations

The main limit to this study was the retrospective placing of ROI on the scans, guided by pathological results. Not only might this have induced a bias in measurement of perfusion parameters, but it also implied that the pathological (3  $\mu\text{m}$  thickness) and CT (3 mm thickness) slices were exactly at the same level. After dissection, the liver did not maintain its *in vivo* position. It was therefore difficult to choose the level of the pathological slice, but we were guided by the portal vein's position, since it was short and nearly in an axial plane.

To test the appropriateness of our methods, we first placed ROI randomly on the liver parenchyma, without prior knowledge of pathological results, on the right, middle and left lobe of the liver. Their mean perfusion parameters were not statistically different from controls. This seemed to indicate that our positioning of ROI on CT, oriented by pathology, indeed reflected the presence of specific lesions. A parametric imaging method is being developed in our laboratory to obtain perfusion parameters in all pixels of the liver. This would allow us to detect focal changes in perfusion without needing to know beforehand where the abnormal areas of liver are. It would also be possible to conduct a prospective study, which would allow a more objective evaluation of the technique's capabilities.

Another limit was that we had no reference method to evaluate vascularization, for example, anti-CD34 or factor VIII staining. We therefore had no way to control that the observed changes in perfusion parameters were indeed correlated with a specific pathological change in vessels. However, as stated earlier, our results are consistent with modifications that have been observed in this model, in particular in Yamamoto's study [14].

This mathematical model is the only model so far that can characterize liver perfusion by six parameters, namely liver perfusion index, MTT, LDV and total, arterial and portal blood flows. This model could be applied in

part because our contrast agent was a macromolecule and diffusion through tumoral capillaries could be neglected over the short time period of observation. However, functions used for fits do not cover extreme situations such as, for example, a totally arterialized input. Also, HPI, though one of the most statistically significant parameters, presented large standard deviations, potentially limiting its use when considering an individual result.

In this study, only one slice was explored, since the CT scan was single slice. Multi-slice scans will allow a complete exploration of the liver, though its use might be restricted in humans by radiation dose limitations.

### Clinical application

The next step is to apply this method to human liver pathology. Applying this mathematical model using MRI instead of CT could circumvent the issue of radiation. Macromolecular contrast agents are also necessary to detect changes in distribution volume. Pharmaceutical companies are developing such molecules, but they are not currently approved for use in humans. However, the main limit to the application of this technique to early detection of HCC in humans is that HCC in Western countries mainly occurs in cirrhotic patients. In cirrhosis, there are also perfusion changes, and liver tissue is often very heterogeneous. It could be difficult to distinguish specific changes resulting from HCC amid all the other changes. A study applying this technique of perfusion CT on cirrhotic patients would have to be carried out prior to any study on HCC. This technique has also been applied to micrometastases in rats, [7] and this could also be a disease explored in humans.

In conclusion, this technique is sensitive and specific, and also non-invasive, since it only requires an intravenous injection of contrast agent. It could be applied to other liver diseases such as metastasis or cirrhosis. A technique such as perfusion CT, quantifying perfusion and reflecting focal changes of vascularization, could allow a reproducible *in vivo* method that could be repeated in the same individual to monitor the biological effects of anti-angiogenic compounds on tumoral vessels.

**Acknowledgment** L.S. Fournier was supported by a grant from the Fondation pour la Recherche Medicale.

### References

1. Palma LD (1998) Diagnostic imaging and interventional therapy of hepatocellular carcinoma. *Br J Radiol* 71:808-818
2. Trojan J, Schroeder O, Raedle J, Baum RP, Herrmann G, Jacobi V, Zeuzem S (1999) Fluorine-18 FDG positron emission tomography for imaging of hepatocellular carcinoma. *Am J Gastroenterol* 94:3314-3319
3. Ramsey WH, Wu GY (1995) Hepatocellular carcinoma: update on diagnosis and treatment. *Dig Dis* 13:81-91



4. Passe TJ, Bluemke DA, Siegelman SS (1997) Tumor angiogenesis: tutorial on implications for imaging. *Radiology* 203:593–600
5. Genecin P, Groszmann RJ (1991) Hepatic blood flow, measurement, and physiological regulation. In: McIntyre N, Benhamou JP, Bircher J (eds) *Oxford textbook of clinical hepatology*. Oxford University, Oxford, pp 31–37
6. Williams GM, Gebhardt R, Sirma H, Stenback F (1993) Non-linearity of neoplastic conversion induced in rat liver by low exposures to diethylnitrosamine. *Carcinogenesis* 14:2149–2156
7. Cuenod C, Leconte I, Siauve N, Resten A, Dromain C, Poulet B, Frouin F, Clement O, Frija G (2001) Early changes in liver perfusion caused by occult metastases in rats: detection with quantitative CT. *Radiology* 218:556–561
8. Travis CC, McClain TW, Birkner PD (1991) Diethylnitrosamine-induced hepatocarcinogenesis in rats: a theoretical study. *Toxicol Appl Pharmacol* 109:289–304
9. Cuenod C, Leconte I, Siauve N, Frouin F, Dromain C, Clement O, Frija G (2002) Deconvolution technique for measuring tissue perfusion by dynamic CT: application to normal and metastatic liver. *Acad Radiol* 9:S205–S211
10. Idee J, Port M, Robert P, Raynal I, Prigent P, Dencausse A, Le Greneur S, Tichkowsky I, Le Lem G, Bourrinet P, Mugel T, Benderbous S, Devoldere L, Bourbouze R, Meyer D, Bonnemain B, Corot C (2001) Preclinical profile of the monodisperse iodinated macromolecular blood pool agent P743. *Invest Radiol* 36:41–49
11. Wiart M, Corot C, Berthezene Y, Violas X, Canet E (2001) CT pulmonary angiography with a macromolecular contrast medium: a comparative study versus iobitridol in rabbits. *Invest Radiol* 36:547–553
12. Conway JG, Popp JA, Thurman RG (1985) Microcirculation of hepatic nodules from diethylnitrosamine-treated rats. *Cancer Res* 45:3620–3625
13. Materne R, Annet L, Dechambre S, Sempoux C, Smith AM, Corot C, Horsmans Y, Van Beers BE (2002) Dynamic computed tomography with low- and high-molecular-mass contrast agents to assess microvascular permeability modifications in a model of liver fibrosis. *Clin Sci* 103:213–216
14. Yamamoto T, Kaneda K, Hirohashi K, Kinoshita H, Sakurai M (1996) Sinusoidal capillarization and arterial blood supply continuously proceed with the advance of the stages of hepatocarcinogenesis in the rat. *Jpn J Cancer Res* 87:442–450
15. Yamaguchi R, Yano H, Nakashima Y, Ogasawara S, Higaki K, Akiba J, Hicklin DJ, Kojiro M (2000) Expression and localization of vascular endothelial growth factor receptors in human hepatocellular carcinoma and non-HCC tissues. *Oncol Rep* 7:725–729
16. Yamaura H, Sato H (1974) Quantitative studies on the developing vascular system of rat hepatoma. *J Natl Cancer Inst* 53:1229–1240
17. Kojiro M, Nakashima O (1999) Histopathologic evaluation of hepatocellular carcinoma with special reference to small early stage tumors. *Semin Liver Dis* 19:287–296